Using scaled FE solutions for an efficient coupled electromagnetic–thermal induction machine model

Martin Marco Nell, Benedikt Groschup and Kay Hameyer
Institute of Electrical Machines (IEM), RWTH Aachen University, Aachen, Germany

Received 13 January 2020
Revised 3 August 2020
Accepted 5 November 2020

Abstract

Purpose – This paper aims to use a scaling approach to scale the solutions of a beforehand-simulated finite element (FE) solution of an induction machine (IM). The scaling procedure is coupled to an analytic three-node-lumped parameter thermal network (LPTN) model enabling the possibility to adjust the machine losses in the simulation to the actual calculated temperature.

Design/methodology/approach – The proposed scaling procedure of IMs allows the possibility to scale the solutions, particularly the losses, of a beforehand-performed FE simulation owing to temperature changes and therefore enables the possibility of a very general multiphysics approach by coupling the FE simulation results of the IM to a thermal model in a very fast and efficient way. The thermal capacities and resistances of the three-node thermal network model are parameterized by analytical formulations and an optimization procedure. For the parameterization of the model, temperature measurements of the IM operated in the 30-min short-time mode are used.

Findings – This approach allows an efficient calculation of the machine temperature under consideration of temperature-dependent losses. Using the proposed scaling procedure, the time to simulate the thermal behavior of an IM in a continuous operation mode is less than 5 s. The scaling procedure of IMs enables a rapid calculation of the thermal behavior using FE simulation data.

Originality/value – The approach uses a scaling procedure for the FE solutions of IMs, which results in the possibility to weakly couple a finite element method model and a LPTN model in a very efficient way.

Keywords Electrical machine, Thermal analysis, Finite element analysis, Coupled systems, Evolution strategies

Paper type Research paper

1. Introduction

The heating up of an induction machine (IM) mainly depends on the ohmic and ferromagnetic losses of the machine. These losses, especially the ohmic losses of the stator winding and the ohmic rotor losses of a squirrel cage IM, are highly temperature dependent, owing to the temperature dependency of their electrical and magnetic properties. Because of this bidirectional connection between electromagnetic losses and temperatures within the electrical machine, electromagnetic and thermal simulations have to be coupled in thermal machine simulations. The coupling can take place in different ways such as numerically strong or weak coupling. On the one hand, the numerically strong coupling is the full coupling of the thermal and electromagnetic fields by describing them with a differential equation system (Hameyer *et al.*, 1999). These equations, describing all modeled effects, are solved simultaneously. The benefit of this method is a high precision, whereas the drawback is a high computational effort. One the other hand, the numerically weak coupling is a cascade and iterative process, where the considered field problems are solved in separated steps (Hameyer *et al.*, 1999). The coupling is given by updating the coupled input parameters

COMPEL - The international journal for computation and mathematics in electrical and electronic engineering
Vol. 40 No. 2, 2021
pp. 267-279

0332-1649
DOI 10.1108/COMPEL-01-2020-0019

of the different fields. In a weak coupled model, it is possible to model the separated fields with models of different precision and computational effort.

With regard to the simulation of the thermal machine behavior, analytical and lumped parameter thermal network (LPTN) models are often used in weakly coupled electromagnetic–thermal simulations. The electromagnetic simulation is often carried out with numerical methods such as the finite element method (FEM). Coupling analytical or equivalent circuit models of the electromagnetic field with LPTN models, as it is performed in Puranen and Pyrhönen (2006), Alberti and Bianchi (2008), Popova *et al.* (2011), Emmrich *et al.* (2014) and Laidoudi *et al.* (2019) results in very low computational effort. The drawback of this method is that the electromagnetic model does not consider the local loss distribution in the machine, which has a very high influence on the simulated overall losses as it is shown in (Von Pfingsten *et al.*, 2017). Furthermore, losses owing to physical effects, such as the slotting or skin effect, are not considered adequately in those analytical electromagnetic models. In contrast to this, the weak coupling of the thermal models with an electromagnetic FEM model enables more precise loss modeling. In Mezani *et al.* (2005), Jiang and Jahns (2013) and Hruska *et al.* (2014), a LPTN model is coupled to an electromagnetic FEM simulation in the form of a weak coupling solving the thermal and electromagnetic problem in an iterative and cascade process. In every iteration step, the FEM simulation is conducted using the actual temperature-dependent conductivities of the stator and rotor winding. Thus, the input losses of the thermal model are updated at every iteration step. The higher precision of the electromagnetic model is gained at the price of higher modeling and calculation effort. One way to reduce this high calculation effort is to reduce the number of updates of the input losses. Because the electromagnetic time constant is much smaller than the thermal one, a reduction of the loss updates is possible. Another possibility is introduced in this paper. The solutions, particularly the losses, of a beforehand-performed FE simulation are scaled according to the actual machine temperature. The FEM simulation has only to be carried out for the first step of the iteration. In the following steps, the scaling approach is used to update the losses of the machine. This enables the possibility to couple the FE simulation results of an IM to a LPTN model in a very fast and efficient way without reducing the number of update steps. The paper presents the specific electromagnetic–thermal coupling model and the scaling laws of the IM regarding temperature changes introduced in Nell *et al.* (2019) more detailed. Furthermore, thermal measurements of exemplary IMs are performed. These measurements are used to parametrize a low-order LPTN model of the machine. Simulations using the presented electromagnetic–thermal coupling approach are validated by comparing the results with the measurement results. In a last step, the importance of the coupling and updating of the temperature-dependent machine losses, respectively, in thermal simulations are shown.

2. Electromagnetic–thermal coupling model

In this paper, a weakly coupled electromagnetic–thermal model is used. The thermal behavior of the IM is modeled using a LPTN. The input of this LTPN is the electromagnetic machine losses $\boldsymbol{P}_{\mathbf{L}}$, i.e. the ohmic losses of the stator winding, the ohmic losses of the rotor winding and the iron losses of the stator and rotor. Owing to the temperature dependency of the electrical conductivity $\sigma_{\mathrm{s}}(\vartheta)$ and $\sigma_{\mathrm{r}}(\vartheta)$ of the stator and rotor winding, the ohmic losses of the stator $P'_{\mathrm{L,ohm,s}}(\vartheta)$ and rotor $P'_{\mathrm{L,ohm,r}}(\vartheta)$ are dependent on the temperature. In this paper, the iron losses are assumed to be temperature independent. To consider the temperature dependency of the ohmic losses, a weak coupling as shown in Figure 1 is used. In every iteration step, the input parameters of the LPTN, which are the losses $\boldsymbol{P}_{\mathbf{L}}(\vartheta)$, are updated. For the loss calculation in the first step (step = 0), a FEM simulation is conducted

for the initial temperature ϑ_0. For the loss update in the following steps, the FEM simulation results of the first step are scaled owing to the actual temperature ϑ. The influence of the temperature on the electromagnetic losses is shown in detail in Section 4. The scaling approach itself provides nearly the same results than a new FEM simulation as it is shown in this paper. As a result, the weak coupling using the scaling laws of the IM enables an efficient way to couple an electromagnetic FEM model with a LPTN model. The simulations in the paper are performed once using this weakly coupled electromagnetic–thermal model by rescaling the machine losses in every iteration step and once without rescaling the losses. The simulation without rescaling of the losses is no longer coupled. It uses constant machine losses during the thermal simulation, which are extracted from one electromagnetic FEM simulation with a certain given temperature.

3. Studied induction machines

The studied IMs are designed as traction drives for small electric vehicles. They are extracted from two-series production batches with five individual machines in each batch. The IMs have a stator outer diameter of $d_{s,a} = 175$ mm, a rotor outer diameter of $d_{r,a} = 102.5$ mm and an axial length of $l_{Fe} = 200$ mm. The rotor outer diameters as well as the stator inner diameters of the machines are measured. Using those measured parameters, the air gap of each of the 10 machines is calculated. The average air gap width of the machines is $l_\delta = 0.48$ mm. All air gap widths are in a tolerance band of $\pm 3.2\%$. The number of pole pairs is $p = 2$ and the number of poles per pole and phase is $q = 3$. The rotors of the machines have 28 deep rotor bars of class B. The IMs are operated with a DC link voltage of $V_{dc} = 130$ V and a maximum inverter current of $I_{inv,max} = 300$ A. The cross-sectional area and parameters of the studied IMs are shown in Figure 2. The housing of the IM is an aluminum cast with cooling fins and the machine is cooled by a forced flow of air tangentially around the cooling fins.

4. Scaling laws of induction machines

In Nell *et al.* (2018a), an approach to scale the FE solutions of IMs considering geometric variations and variations in temperature is proposed. This scaling approach is used in this

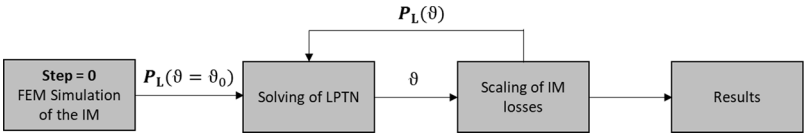

Figure 1. Flowchart of the electromagnetic–thermal coupling analysis of the IM

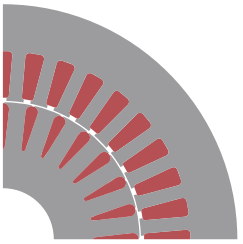

number of pole pairs	p	2
stator outer diameter	$d_{s,a}$	175.0 mm
rotor outer diameter	$d_{r,a}$	102.5 mm
air gap length	l_δ	0.48 mm
axial iron length	l_{Fe}	200.0 mm
number of stator teeth	N_s	36
stator tooth width	$w_{s,T}$	19.7 mm
stator yoke height	$w_{s,Y}$	17.6 mm
number of rotor teeth	N_r	28
rotor tooth width	$w_{r,T}$	17.0 mm
rotor yoke height	$w_{r,Y}$	14.98 mm

Figure 2. Cross-sectional area and machine data of the studied IM

paper to show the influence of temperature variations in the simulation of IMs and to update the input losses of the thermal machine model in the weakly coupled electromagnetic–thermal simulation.

4.1 Temperature scaling of the stator resistance

The stator resistance is evaluated in the post processing routine of a stator current-driven IM FE simulation. The stator resistance R_s is described by:

$$R_s = 2N_s \frac{l_{Fe} + l_{WH}}{\sigma_s A_{wire}}, \tag{1}$$

where l_{WH} is the length of the end winding, l_{Fe} is the axial length of the stator iron package, A_{wire} is the wire cross-sectional area, σ_s is the conductivity of the winding material and N_s is the number of stator slots.

The temperature changes in the stator winding can be considered by recalculating the stator resistance R_s using:

$$R_s' = R_s \cdot \left(1 + \alpha\left(\vartheta_{sim,new} - \vartheta_{ref}\right)\right) . \tag{2}$$

Here, α is the temperature coefficient of the stator winding material, $\vartheta_{sim,new}$ is the new simulated stator temperature and ϑ_{ref} is the reference temperature. The scaled stator resistance R_s' leads to scaled ohmic losses of the stator:

$$P_{L,ohm,s}' = 3 \cdot I_s^2 \cdot R_s', \tag{3}$$

which are used as an input in the LPTN model of the IM in Figure 8.

4.2 Temperature scaling of the rotor resistance

4.2.1 Rotor resistance in the 2D-finite element method simulation. The rotor resistance R_r of an IM has a significant impact on the machine's behavior. Variations in temperature influence the rotor resistance and, therefore, have to be considered when analyzing the IM. The rotor resistance consists of two parts. The first part is the electrical resistance of the rotor bar:

$$R_{bar} = \frac{l_{Fe}}{\sigma_r A_{bar}}, \tag{4}$$

where l_{Fe} is the active magnetic length of the IM, A_{bar} is the area of a rotor bar and σ_r is the conductivity of the rotor conductors. The second part is the resistance of the short-circuit ring. The resistance of a short-circuit ring segment ΔR_{ring} can be described by:

$$\Delta R_{ring} = \frac{2\pi r_{ring}}{\sigma_r A_{ring} Q_r}, \tag{5}$$

where r_{ring} describes the middle radius of the short-circuit ring, A_{ring} is the cross-sectional area of the short-circuit ring and Q_r is the number of the rotor bars. In the 2D FEM simulation, the resistance of the short-circuit ring has to be transformed to an equivalent series resistance ΔR_{ring}^* that is added to the rotor bar resistance. According to

Nell *et al.* (2018a) and equation (12) in Williamson and Begg (1986), this equivalent series resistance of the short-circuit ring can be calculated by:

$$\Delta R^{*}_{\mathrm{ring}} = \Delta R_{\mathrm{ring}} \cdot \frac{1}{\left(2\sin\left(\frac{\pi p}{Q_{\mathrm{r}}}\right)\right)^{2}}, \tag{6}$$

with the number of pole pairs p. The addition of the bar resistance and the equivalent series resistance of the short-circuit ring leads to the total resistance of the rotor:

$$R_{\mathrm{r}} = R_{\mathrm{bar}} + 2\Delta R^{*}_{\mathrm{ring}} \ . \tag{7}$$

In contrast to the stator resistance, the rotor resistance R_{r} is defined in the preprocessing of the 2D FEM simulation in the form of a compensating conductivity. This compensating conductivity $\sigma_{\mathrm{r,comp}}$ is described by:

$$\sigma_{\mathrm{r,comp}} = \frac{l_{\mathrm{Fe}}}{A_{\mathrm{bar}} R_{\mathrm{r}}} \ . \tag{8}$$

4.2.2 Rotor resistance scaling due to rotor conductivity variations. The scaling of the rotor resistance in accordance to the scaling of the compensating rotor conductivity leads to further possibilities of rotor resistance scaling. The rotor conductivity and resistance respectively can vary owing to a variation of the material or the temperature (Nell *et al.*, 2018a). The temperature variation of the rotor cage and rotor conductivity, respectively, can be considered by the second rotor resistance scaling factor:

$$k_{\mathrm{R2}} = \frac{\sigma_{\mathrm{r}}}{\sigma_{\mathrm{r,new}}} \cdot \frac{1 + \alpha_{\mathrm{new}}\left(\vartheta_{\mathrm{sim,new}} - \vartheta_{\mathrm{ref,new}}\right)}{1 + \alpha(\vartheta_{\mathrm{sim}} - \vartheta_{\mathrm{ref}})}, \tag{9}$$

introduced in Nell *et al.* (2018a). It is dependent on the old and new conductivity, σ_{r} and $\sigma_{\mathrm{r,new}}$, the old and new temperature coefficients α and α_{new}, the old and new reference temperatures ϑ_{ref} and $\vartheta_{\mathrm{ref,new}}$ and the old and new simulation temperatures ϑ_{sim} and $\vartheta_{\mathrm{sim,new}}$. By neglecting the other scaling possibilities in Nell *et al.* (2018a), such as geometric scaling, the temperature change in the rotor cage yields the scaled rotor resistance:

$$R'_{\mathrm{r}} = R_{\mathrm{r}} \cdot k_{\mathrm{R2}} \tag{10}$$

and the scaled ohmic losses of the rotor:

$$P'_{L,\mathrm{ohm,r}} = P_{L,\mathrm{ohm,r}} \cdot k_{\mathrm{R2}}, \tag{11}$$

that are used as an input in the LPTN model of the IM in Figure 8.

4.2.3 Scaling of the finite element -simulation results of the induction machine due to temperature variations. In Nell *et al.* (2018a), the approach to scale the results of the FE simulation of an IM is proposed. The machine is simulated in the stator-current-slip-frequency operation plane ($I_{\mathrm{s}} - f_{\mathrm{r}} -$ plane) holding the stator frequency f_{s} constant. The scaling in Nell *et al.* (2018a) is also done in the $I_{\mathrm{s}} - f_{\mathrm{r}} -$ plane showing a very good agreement with the simulation results of a pre-scaled machine. One boundary condition that must be

fulfilled when scaling the FE solutions of the IM is that the field strength in the machine must not change during the scaling process (Nell *et al.*, 2018a). Therefore, the time and frequency in the $I_s - f_r -$ plane have to be scaled by a time scaling factor k_t introduced in Nell *et al.* (2018a). Neglecting the geometric scaling of the machine this time scaling factor k_t is reduced to

$$k_t = \frac{1}{k_{R2}} \quad . \tag{12}$$

The results in the $I_s - f_r -$ plane are transformed to the torque-speed map ($T - n -$ map) by scaling the iron losses according to the speed n. In addition, the comparison of the scaled FE simulation results and the results of the pre-scaled machine in the $T - n -$ map show a good agreement. Therefore, scaling laws for scaling the IM in the $I_s - f_r -$ plane and the $T - n -$ map are derived. To compare the scaling of the machine owing to temperature variations in the $I_s - f_r -$ plane and the $T - n -$ map machine simulations are performed and compared in this paper. The first simulation is performed for a stator and rotor temperature of 25°C and the second FE simulation is performed with a stator and rotor temperature of 100°C. The difference in the efficiency for the studied IM at 25°C and 100°C is shown in Figure 3. In the base speed region, the difference is higher than 2%, whereas in the field weakening range at low torques, the difference is less than 1%. The results of the FE simulation at 25°C are scaled to a temperature of 100°C, ones scaled in the $I_s - f_r -$ plane and then transformed to the $T - n -$ map and ones directly in the $T - n -$ map. The efficiency maps of the simulated machine at 100°C and the machine scaled from 25°C to 100°C are compared. By scaling the machine in the $I_s - f_r -$ plane, the maximum efficiency deviation in the entire operating area is 0.12%. The deviation by scaling the machine directly in the $T - n -$ map is higher and shown in Figure 4. The slightly larger error is owing to the error tolerance of the iron loss scaling with respect to the speed described in von Pfingsten *et al.* (2017).

5. Temperature measurements of the induction machine

Temperature measurements of all 10 IMs are performed on the test bench. The setup of the test bench is shown in Figure 5. For the measurement of the electrical quantities, a torque transducer, current transformers and a power analyzer Yokogawa WT 3000 is used. To measure the average stator winding temperature $\vartheta_{winding}$, seven temperature sensors are used at different positions inside the winding. To measure the rotor temperature ϑ_{rotor}, a noncontact infrared (IR) temperature measurement on the surface of the short-circuit ring is used. The rotor surface is spray painted black to create a non-reflecting surface at IR, i.e. an IR emissivity > 0.97 (von Pfingsten *et al.*, 2017). The validation of the IR temperature

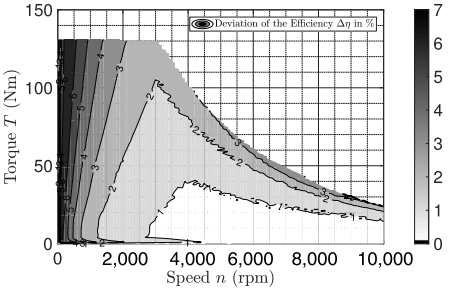

Figure 3.
Absolute difference of the efficiency between a machine temperature of ϑ = 25°C and ϑ = 100°C ($\eta_{\vartheta=25°C} - \eta_{\vartheta=100°C}$)

measurement of the rotor temperature is done using a second machine equipped with four Pt-100 temperature sensors in the rotor cage and a rotor telemetry system (von Pfingsten *et al.*, 2017).

For the temperature measurements, the machines are operated in the 30-min short-time mode at four different speed torque operating points. The operating points are at a torque $T = 60$ Nm and a speed $n = 1{,}900$ rpm, at $T = 60$ Nm and $n = 3{,}700$ rpm, $T = 37$ Nm and $n = 5{,}700$ rpm and $T = 26$ Nm and $n = 7{,}500$ rpm. Exemplary measurement results of the stator winding and the rotor temperatures of the 10 studied IMs operated at $T = 60$ Nm and $n = 1{,}900$ rpm are shown in Figures 6 and 7, respectively.

6. Thermal model of the induction machine

To simulate the thermal behavior of the IMs, the three-node LPTN model in Figure 8 is used. Its inputs are the FE-calculated rotor losses $P_{\mathrm{L,r}}$, which are the sum of the ohmic rotor losses $P_{\mathrm{L,ohm,r}}$ and the rotor iron losses $P_{\mathrm{L,Fe,r}}$, the ohmic stator losses $P_{\mathrm{L,ohm,s}}$ and the stator iron losses $P_{\mathrm{L,Fe,s}}$. Node 1 represents the rotor including the shaft, rotor cage and bearings, node 2 the stator winding and node 3 the stator, including the lamination and the housing of the machine. The nodes are connected by a thermal resistance representing the temperature difference caused by the passed heat flow. The thermal resistances are the thermal air gap resistance R_δ, the thermal resistance between the stator winding and the stator iron $R_{\mathrm{s,Cu-Fe}}$ and the thermal resistance between the stator and the ambient $R_{\mathrm{s,Fe\text{-}Amb}}$. The ambient temperature T_{Amb} is held constant in the simulations and has a value of $T_{\mathrm{Amb}} = 25°\mathrm{C}$. As thermal capacities, the thermal capacity of the stator winding $C_{\mathrm{s,Cu}}$, the thermal capacity of the stator iron, including the housing and the bearing shields, $C_{\mathrm{s,Fe}}$ and the thermal capacity of the rotor C_{r} are used.

For the parametrization of the thermal model, analytic calculations and an evolutionary optimization strategy as described in Nell *et al.* (2018b) are applied. The thermal air gap resistance R_δ is calculated analytically according to the approach in Pyrhönen *et al.* (2008). The thermal capacity of the stator winding $C_{\mathrm{s,Cu}}$ is calculated by using the mass of the copper winding and its specific thermal capacity. The specific thermal capacity of the rotor is the sum of the thermal capacities of the rotor iron, the rotor cage and the shaft. Each capacity is calculated. As a result, the total thermal rotor capacity is calculated to 6.12 kJ/K. To consider initially neglected materials such as the baking varnish between the steel sheets or inaccuracies in the calculation, the parameter is tolerated with $\pm 10\%$. Because the thermal capacity of the stator $C_{\mathrm{s,Fe}}$ could not be calculated exactly, upper and lower limits of this value are defined and set to realistic values. The lower limit is estimated by considering only the stator lamination and the upper limit by considering the estimated capacity of the

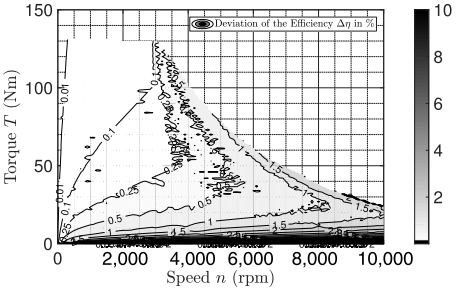

Figure 4.
Absolute difference of the efficiency between a machine scaled from $\vartheta = 25°\mathrm{C}$ to $\vartheta = 100°\mathrm{C}$ in the $T - n$ – map and a machine simulated at $\vartheta = 100°\mathrm{C}$ ($\eta_{\mathrm{scaled},\vartheta=100°\mathrm{C}} - \eta_{\vartheta=100°\mathrm{C}}$)

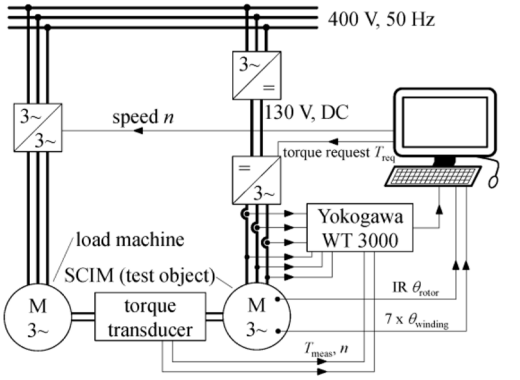

Source: Von Pfingsten et al. (2017)

Figure 5.
Test bench setup of the studied IM

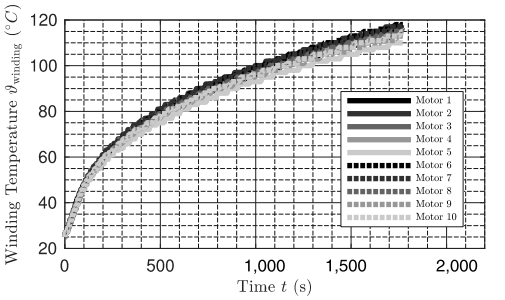

Figure 6.
Measured stator winding temperature of the studied 30-min short-time operation mode at $T = 60$ Nm and $n = 1{,}900$ rpm

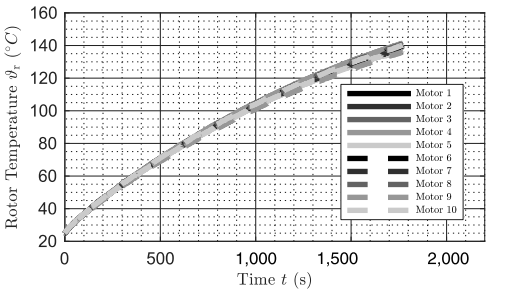

Figure 7.
Measured rotor temperature of the studied 30-min short-time operation mode at $T = 60$ Nm and $n = 1{,}900$ rpm

stator lamination, the housing and the bearing shields. The remaining thermal resistances are calculated by using the thermal heat transfer coefficients. Because there are many unknown parameters for these resistances, upper and lower limits according to Pyrhönen *et al.* (2008) are used. The lower and upper limits for the heat transfer coefficient from the winding to the stator iron $\alpha_{s,Cu-Fe}$ and from the stator iron to the ambient $\alpha_{s,Fe-Amb}$ and for the other variable parameters are shown in Table 1.

The optimization procedure used for the parameterization of the thermal IM model is performed based on the measured temperatures during the 30 – min short-time operation mode. As already mentioned, the optimization process uses the evolutionary strategy based

on Rechenberg (1984) and Schwefel (1995), discussed in Nell *et al.* (2018b) and Nell *et al.* (2018a). For the objective function J of the evolutionary strategy, the sum of the variance of the simulated and the measured rotor and stator winding temperatures:

$$J = \sqrt{\frac{1}{N} \cdot \sum_{i=1}^{N} \left(\vartheta_{\text{winding,sim}} - \vartheta_{\text{winding,meas}}\right)^2} + \sqrt{\frac{1}{N} \cdot \sum_{i=1}^{N} \left(\vartheta_{\text{r,sim}} - \vartheta_{\text{r,meas}}\right)^2}, \tag{13}$$

evaluated in a transient analysis at N intervals of 30 s is used. The parameterization as well as the simulations in this paper are performed by using the operating point at a torque of $T = 60$ Nm and a speed of $n = 1{,}900$ rpm. In this operating point, the difference between a cool and a warm machine is sufficiently high as described in Section 4.2.3, so that the influence of the thermal machine simulation with and without rescaling the losses owing to temperature change is visible. The parameterization is done two times. Once using the temperature-scaled losses of the FE simulation as the input parameters of the model described in Section 2 and once using the unscaled parameters. For the unscaled input parameters, a FE simulation at a rotor and stator temperature of 100°C is conducted. The resulting data of the parameterizations are listed in Table 1.

7. Calculation of the induction machines thermal behavior using the weakly coupled model

The temperature behavior of the exemplary IM is simulated once using the proposed weakly electromagnetic thermally coupled model that rescales and updates the temperature-dependent losses and once without the coupling, rescaling and updating process. In Figure 9, the measured stator winding temperature, the simulated temperature without rescaling and the simulated temperature with rescaling the input parameters of the thermal machine model are shown. The temperature profile simulated with rescaling using the proposed weakly electromagnetic thermally coupled model is in very good agreement with the measured temperatures. The temperature profile simulated without coupling and rescaling, respectively, shows a slightly worse agreement. For temperatures below 100°C,

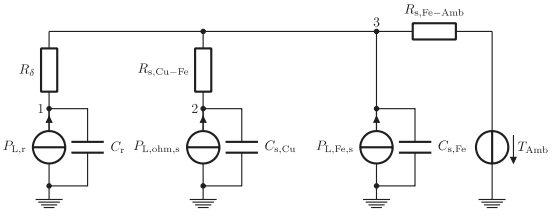

Figure 8.
Thermal three-node model of the IM

Variable	Unit	Lower limit	Upper limit	Calculated data with rescaling the losses	Calculated data without rescaling the losses
Cr	kJ/K	5.51	6.73	6.48	6.59
Cs,Fe	kJ/K	11.78	13.6	12.65	13.30
αs,Fe-Amb	W/(m^2 K)	25	250	112.3	101.6
αs,Cu-Fe	W/(m^2 K)	10	100	51.1	56.9

Table 1.
Boundary conditions and results of parameter identification with rescaling the losses

the simulated temperature is a little bit higher than the measured one and for temperatures above 100°C, the temperature is a little bit lower. Also, it tends to underestimate the temperature after 30 min. In Figure 10, the measured rotor temperature, the simulated temperature without rescaling and the simulated temperatures with rescaling the input parameters of the thermal machine model are shown. The temperature profile simulated with rescaling and the profile simulated without rescaling show a good agreement to the measured temperature. For temperatures below 100°C, the simulated temperatures with rescaling are a little bit lower than the measured one and the simulated temperatures without rescaling a little bit higher. For the time after 30 min, the temperature simulated with rescaling tends to be higher than the one simulated without rescaling the input parameters of the thermal model.

8. Calculation of induction machines thermal behavior considering temperature-dependent losses

With the parametrized thermal three-node model of the IM, a continuous operation of the machine with a torque of $T = 60$ Nm and a speed of $n = 1{,}900$ rpm is simulated once without rescaling the FE solutions of the machine owing to a temperature change and once with rescaling the FE solutions. For this, the thermal three-node model is solved in intervals of 30 s. For the weakly coupled simulation with rescaling, the input parameters of the model are updated in every simulation step. The resulting winding temperatures and rotor temperatures are shown in Figure 11. As discussed in Section 7, the temperature of the winding and rotor simulated with and without rescaling the machine losses agree well for the first 1,800 s. After a time of 1,800 s, the simulated temperature with and without rescaling diverge. At 1,800 s, the winding temperature simulated with rescaling of the input parameters is $\vartheta = 139$°C and $\Delta\vartheta = 15$°C higher than for the simulation without rescaling. The rotor temperature with the

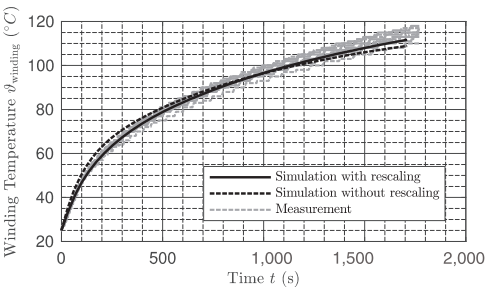

Figure 9.
Measured and simulated winding temperature of the studied 30-min short-time operation mode at $T = 60$ Nm and $n = 1{,}900$ rpm

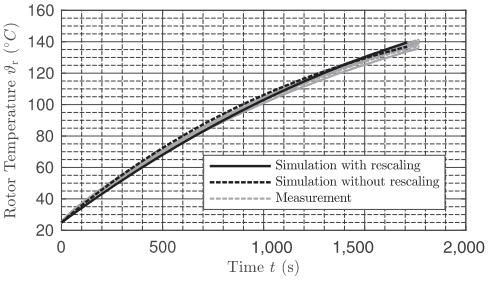

Figure 10.
Measured and simulated rotor temperature of the studied 30-min short-time operation mode at $T = 60$ Nm and $n = 1{,}900$ rpm

rescaling process at 8,000 s reaches a value of $\vartheta = 214°C$. This temperature is $\Delta\vartheta = 36°C$ higher than the temperature simulated without the rescaling process.

The difference in temperature is caused by the increasing losses and thus decreasing efficiency when heating up the machine. In Figure 12, the efficiency and the ohmic stator and rotor losses simulated with the weakly coupled electromagnetic–thermal machine model for the given operating point are shown with solid lines. In dashed lines, the efficiency, ohmic stator and ohmic rotor losses for the temperature of $\vartheta = 100°C$, which is used in the non-coupled simulation without rescaling the losses are shown. The increase of the ohmic stator losses of about 45% and the ohmic rotor losses of about 70% show the origin of the temperature differences in Figure 11 and the importance of coupling the electromagnetic and thermal simulation.

9. Conclusions and further work

One way to consider the bidirectional connection of electromagnetic losses and temperatures of IMs in the analysis of its thermal behavior is to use a weakly coupled electromagnetic–thermal machine model. Coupling LPTN models and electromagnetic FE models promises thereby accurate results in terms of the electromagnetic losses and temperatures. The drawback of this method is the high computational effort owing to conducting the electromagnetic FE simulation in every iteration of the weakly coupled simulation. To overcome this high computational effort without reducing the accuracy of the electromagnetic loss calculation, a scaling procedure to scale the FE simulation results of IMs is used. This approach enables the coupling of the electromagnetic FEM model and the LPTN model in a very efficient way. In the paper, the scaling laws of an IM that are used to scale the FE solutions owing to temperature

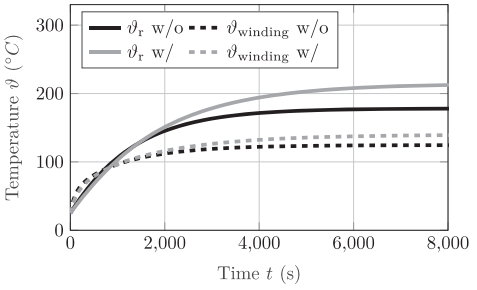

Figure 11.
Results of the temperature simulation with (w/) and without (w/o) rescaling of the FE solutions of the IM

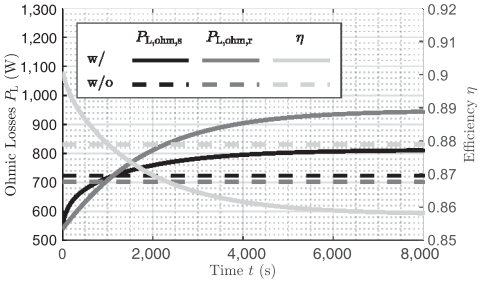

Figure 12.
Ohmic stator losses, ohmic rotor losses and efficiency during the thermal simulation of the IM using the weakly coupled electromagnetic–thermal simulation model (w/) and using the non-coupled model (w/o)

variations in the stator and rotor are discussed and verified. A parameterization of a three-node LPTN model is performed by analytical formulas and by an optimization procedure. For the optimization procedure, the results of temperature measurements of IMs on the test bench are considered. Thermal simulations with and without using the presented scaling approach show a high influence on the simulated thermal behavior of the IM considering temperature-scaled machine losses or not. Neglecting the temperature dependency of the machine's losses leads to underestimated simulated temperatures in the continuous operation mode of the machine. In further work, the proposed model will be used for multiple operation points of the IM to validate the proposed approach in different conditions. Furthermore, the parameters of the thermal network models will be analyzed in more detail to increase the accuracy of the thermal model. The coupling of the scaling procedure of the FE simulation with a more detailed thermal model will be addressed.

References

Alberti, L. and Bianchi, N. (2008), "A coupled thermal–electromagnetic analysis for a rapid and accurate prediction of IM performance", *IEEE Transactions on Industrial Electronics*, Vol. 55 No. 10, pp. 3575-3582.

Emmrich, K., Brune, A. and Ponick, B. (2014), "Evaluation of an analytical, efficiency-optimized torque-speed characteristic of induction machines coupled with a thermal-electromagnetic energy consumption calculation", *2014 International Conference on Electrical Machines (ICEM), Berlin*, pp. 762-767.

Hameyer, K., Driesen, J., De Gersem, H. and Belmans, R. (1999), "The classification of coupled field problems", *IEEE Transactions on Magnetics*, Vol. 35 No. 3, pp. 1618-1621.

Hruska, K., Kindl, V., Pechanek, R. and Skala, B. (2014), "Evaluation of different approaches of mathematical modelling of thermal phenomena applied to induction motors", *2014 ELEKTRO, Rajecke Teplice*, pp. 358-362.

Jiang, W. and Jahns, T.M. (2013), "Development of efficient electromagnetic-thermal coupled model of electric machines based on finite element analysis", *2013 International Electric Machines and Drives Conference, Chicago, IL*, pp. 816-823.

Laidoudi, A., Duchesne, S., Mgzaizar, M. and Takorabet, N. (2019), "Increase the power-to-weight ratio of induction machines by increasing their operating temperature", *2019 19th International Symposium on Electromagnetic Fields in Mechatronics, Electrical and Electronic Engineering (ISEF), Nancy*, pp. 1-2.

Mezani, S., Takorabet, N. and Laporte, B. (2005), "A combined electromagnetic and thermal analysis of induction motors", *IEEE Transactions on Magnetics*, Vol. 41 No. 5, pp. 1572-1575.

Nell, M., Groschup, B. and Hameyer, K. (2019), "Efficient coupled electromagnetic-thermal induction machine model using scaled FE-solutions", *2019 19th International Symposium on Electromagnetic Fields in Mechatronics, Electrical and Electronic Engineering (ISEF), Nancy*, pp. 1-2.

Nell, M., Lenz, J. and Hameyer, K. (2018a), "Efficient numerical optimization of induction machines by scaled FE simulations", *2018 XIII International Conference on Electrical Machines (ICEM)*, pp. 198-204.

Nell, M., von Pfingsten, G. and Hameyer, K. (2018b), "Rapid parameter identification and control of an induction machine", *COMPEL – The International Journal for Computation and Mathematics in Electrical and Electronic Engineering*, Vol. 37 No. 5, pp. 1678-1688.

Rechenberg, I. (1984), "The evolution strategy – a mathematical model of Darwinian evolution", *Synergetics – From Microscopic to Macroscopic Order*, Vol. 22, pp. 122-132.

Schwefel, H.P. (1995), *Evolution and Optimum Seeking*, Wiley-Verlag.

Popova, L., Nerg, J. and Pyrhönen, J. (2011), "Combined electromagnetic and thermal design platform for totally enclosed induction machines", *8th IEEE Symposium on Diagnostics for Electrical Machines, Power Electronics and Drives, Bologna*, pp. 153-158.

Puranen, J. and Pyrhönen, J. (2006), "Optimization of the loadability of an induction servomotor with a coupled electromagnetic-thermal model", *International Symposium on Power Electronics, Electrical Drives, Automation and Motion, 2006, SPEEDAM*, pp. 153-158.

Pyrhönen, J., Jokinen, T. and Hrabovcová, V. (2008), *Design of Rotating Electrical Machines*. John Wiley and Sons.

Von Pfingsten, G., Steentjes, S. and Hameyer, K. (2017), "Operating point resolved loss calculation approach in saturated induction machines", *IEEE Transactions on Industrial Electronics*, Vol. 64 No. 3, pp. 2538-2546.

Williamson, S. and Begg, M.C. (1986), "Calculation of the resistance of induction motor end rings", *IEE Proceedings B Electric Power Applications*, Vol. 133 No. 2, pp. 54-60.

Further reading

Zhang, Y., Ruan, J., Huang, T., Yang, X., Zhu, H. and Yang, G. (2012), "Calculation of temperature rise in air-cooled induction motors through 3-D coupled electromagnetic fluid-dynamical and thermal finite-element analysis", *IEEE Transactions on Magnetics*, Vol. 48 No. 2, pp. 1047-1050.

About the authors

Martin Marco Nell was born in Koblenz in Germany on July 11, 1990. He received master's degree in April 2017 in Electrical Engineering from RWTH Aachen University, Germany. He has been working as Research Associate at the Institute of Electrical Machines since May 2017. His research interests include induction machine modeling, optimization of induction machines, iron loss calculation in macroscopic scale and vehicle modeling. Martin Marco Nell is the corresponding author and can be contacted at: martin.nell@iem.rwth-aachen.de

Benedikt Groschup was born in Würzburg, Germany on March 13, 1990. He received master's degree in Automotive Engineering and Transport in September 2015 at RWTH Aachen University in collaboration with Ford Motor Company in Detroit, Michigan, USA. He started working as Research Associate of RWTH Aachen University in February 2016. His research interests include induction and permanent magnet motor modeling, iron loss calculation in macroscopic scale, vehicle modeling and thermal modeling.

Kay Hameyer received Master of Science in electrical engineering from the University of Hannover and his PhD from the Berlin University of Technology, Germany. After his university studies, he worked with the Robert Bosch GmbH in Stuttgart, Germany, as Design Engineer for permanent magnet servo motors and vehicle board net components. From 1996 to 2004, Dr Hameyer was Full Professor for Numerical Field Computations and Electrical Machines with the KU Leuven in Belgium. Since 2004, he is Full Professor and Director of the Institute of Electrical Machines (IEM) at RWTH Aachen University in Germany. In 2006, he was Vice Dean of the faculty and from 2007 to 2009, he was Dean of the Faculty of Electrical Engineering and Information Technology of RWTH Aachen University. His research interests are numerical field computation and optimization, the design and controls of electrical machines, in particular permanent magnet excited machines and induction machines. Since several years, Dr Hameyer's work is concerned with magnetically excited audible noise in electrical machines, the lifetime estimation of insulating systems and the characterization of ferromagnetic materials. Dr Hameyer is author of more than 250 journal publications, more than 700 international conference publications and author of four books. Dr Hameyer is a member of VDE, IEEE senior member and fellow of the IET.